Breakup coupling effects on near-barrier quasi-elastic scattering of ^{6,7}Li on ^{144}Sm

D. R. Otomar,[1] J. Lubian,[1,*] P. R. S. Gomes,[1] D. S. Monteiro,[1] O. A. Capurro,[2] A. Arazi,[2] J. O. Fernández Niello,[2,3] J. M. Figueira,[2] G. V. Martí,[2] D. Martinez Heimann,[2] A. E. Negri,[2] A. J. Pacheco,[2] V. Guimarães,[4] and L. C. Chamon[4]

[1]*Instituto de Física, Universidade Federal Fluminense, Av. Litoranea s/n, Gragoatá, Niterói, R. J., 24210-340, Brazil*

[2]*Laboratorio Tandar, Comisión Nacional de Energía Atómica, Av. General Paz 1499, 1650 San Martín, Buenos Aires, Argentina*

[3]*Escuela de Ciencia y Tecnología, Universidad de San Martín, San Martín, 1650 San Martín, Argentina*

[4]*Instituto de Física, Universidade de São Paulo, C. P. 66318, 05389-970 São Paulo, Brazil*

(Received 25 June 2009; published 23 September 2009)

Excitation functions of quasi-elastic scattering at backward angles have been measured for the ^{6,7}Li + ^{144}Sm systems at near-barrier energies, and fusion barrier distributions have been extracted from the first derivatives of the experimental cross sections with respect to the bombarding energies. The data have been analyzed in the framework of continuum discretized coupled-channel calculations, and the results have been obtained in terms of the influence exerted by the inclusion of different reaction channels, with emphasis on the role played by the projectile breakup.

DOI: 10.1103/PhysRevC.80.034614 PACS number(s): 25.70.Mn, 25.70.Bc, 24.10.Eq

I. INTRODUCTION

The role of inelastic excitations and transfer channel couplings on the fusion cross section has been extensively investigated during the last decades. Huge subbarrier fusion enhancements, when compared with no-coupled calculations, were found in several systems, particularly when deformed nuclei were involved. The coupling of different channels gives rise to associated different Coulomb barriers, responsible for the observed behavior of the fusion excitation functions, especially at subbarrier energies.

Rowley proposed [1] a very sensitive method for investigating the role of different couplings on the fusion cross sections at energies around the Coulomb barrier. The method consists in deriving the fusion barrier distributions from very precise fusion excitation functions. The fusion barrier distribution is obtained by the expression [1]

$$D^{\rm fus}(E) = \frac{d^2}{dE^2}[E\sigma^{\rm fus}(E)]. \quad (1)$$

Several works have been published on the derivation and analysis of fusion barrier distributions (see, for instance, Refs. [2,3]). However, in addition to the very precise measurements of fusion excitation functions, this method requires the use of its second derivative with respect to the energy.

Since the channel couplings also affect the scattering process, an alternative procedure for obtaining information about fusion barrier distributions is the derivation of backward angle quasi-elastic scattering barrier distributions [4–6]. Quasi-elastic scattering (QES) is defined as the sum of all direct processes such as elastic and inelastic scattering and transfer reactions. Since fusion is connected with transmission through a barrier and large angle quasi-elastic scattering is connected with reflection at that barrier, because of the conservation of the reaction flux, these two processes may be considered as complementary to each other. Besides, it has been demonstrated [7,8] that the two representations of the barrier distributions are equivalent. Therefore, information about the fusion process may be obtained by QES cross section measurements at backward angles, which in most situations is much simpler to investigate experimentally than fusion. Furthermore, the QES barrier distributions at backward angles are obtained from the first derivative of the quasi-elastic excitation functions [5]

$$D^{\rm fus}(E) = -\frac{d}{dE}\left[\frac{d\sigma^{\rm QES}(E)}{d\sigma^{\rm Ruth}(E)}\right], \quad (2)$$

where $\sigma_{\rm Ruth}$ is the Rutherford cross section, and therefore they may carry lower uncertainties than the distributions derived from fusion.

In the last few years, the influence of the breakup of weakly bound nuclei on fusion cross section has been widely investigated [9]. Since the breakup reaction channel feeds states in the continuum, the role of this process on the fusion and scattering channels is expected to be different from bound-state inelastic excitations and direct transfer reactions. Among others, Dasgupta *et al.* studied fusion barrier distributions involving the weakly bound projectiles ^{6,7}Li and ^{9}Be on heavy targets [10]. However, there are only few preliminary reports [11–14] on the investigation of fusion barrier distributions derived from backward angle QES for systems involving weakly bound nuclei. For such systems, the breakup channel must be included as one of the quasi-elastic processes. Breakup is a very complex channel, since following the projectile fragmentation, the products may have different behaviors. If all pieces fly away from the target, the process is called noncapture breakup (NCBU); if one of the fragments fuses with the target, the process is called incomplete fusion (ICF); if all fragments fuse with the target, the process is called sequential complete fusion (SCF). Therefore, for weakly bound systems, QES is complementary to the complete fusion (CF) of the projectile with the target and includes NCBU and ICF.

The measurements of fusion cross sections for systems with weakly bound projectiles and medium-heavy target masses is

*lubian@if.uff.br

particularly difficult, because the evaporation residues have low energies to pass through a conventional detector window, and they do not decay by either α emission or fission. Fusion cross sections for the ^{9}Be + ^{144}Sm system were measured by our group [15] by the delayed x-ray detection method, but fusion barrier distributions could not be derived. Fusion cross sections measured for the ^{6}Li + ^{144}Sm system using γ-ray spectroscopy has been reported very recently [16]. Although the fusion excitation function was determined by measuring at a relatively small number of different bombarding energies, a simplified fusion barrier distribution was able to be extracted for that system.

In the present paper, we report the measurement of the large-angle partial QES excitation function and the corresponding barrier distribution for the ^{7}Li + ^{144}Sm system, at near-barrier energies. Furthermore, we analyzed these data and previously reported measurements for the ^{6}Li + ^{144}Sm [12] by means of continuum discretized coupled-channel (CDCC) calculations. This is the first calculation of this type reported for QES for which there are experimental data to compare with. For example, in Ref. [12], the experimental partial QES cross sections for the ^{6}Li + ^{144}Sm system were compared with coupled-channel estimates but without the inclusion of the breakup channel. On the other hand, a QES barrier distribution extracted from CDCC calculations involving the proton halo ^{8}B projectile was recently performed by our group for the ^{8}B + ^{58}Ni system [14], which had no available experimental data.

In Sec. II of this paper, we present the experimental setups. In Secs. III and IV, we show the experimental excitation functions and barrier distributions for the ^{7}Li + ^{144}Sm and ^{6}Li + ^{144}Sm systems, respectively, and compare those results with CDCC calculations. In Sec. V, we present a summary of the results and the conclusions.

II. EXPERIMENTAL SETUPS

The experiments were performed at the Tandar Laboratory. Experimental details and results for ^{6}Li + ^{144}Sm have already been reported [12]. As the experimental setup for the ^{7}Li + ^{144}Sm system was similar to the other system, only a brief description will be given in this paper. Beams of ^{6}Li and ^{7}Li were delivered by the tandem accelerator at bombarding energies ranging from 14 to 35 MeV and from 12 to 32 MeV, respectively, corresponding to energies well below to above the Coulomb barrier. For ^{6}Li + ^{144}Sm, energy steps of 1 MeV were used at energies well below and well above the barrier, whereas 0.5 MeV energy steps were used at near-barrier energies. For ^{7}Li + ^{144}Sm, the chosen energy step was 0.5 MeV for energies well bellow and near the Coulomb barrier; for the rest of the energy range, the 1.0 MeV step was used. The terminal voltage was varied monotonically to reduce magnetic hysteresis effects [17]. The beam energy uncertainty was of the order of 0.5% [12]. The target consisted of 88% enriched ^{144}Sm, with 200 μg/cm^2 thickness, evaporated onto a carbon backing. Most of the target impurities come from the ^{147,148,149}Sm isotopes.

The detection system consisted of two ΔE-E telescopes, with thicknesses of 15–150 and 30–150 μm, respectively.

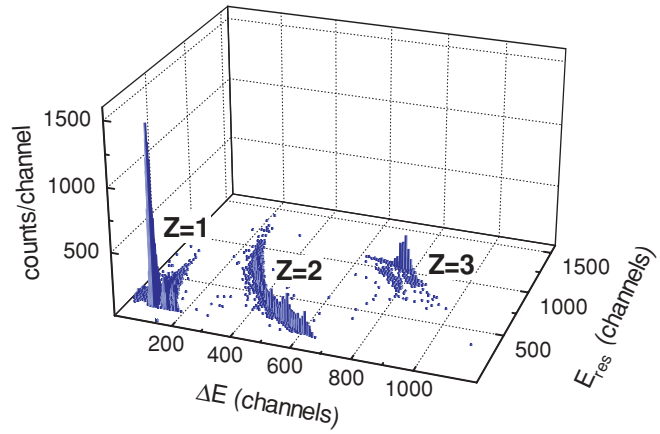

FIG. 1. (Color online) Spectrum for the ^{7}Li + ^{144}Sm system, at $E_{\rm lab} = 27$ MeV and $\theta_{\rm lab} = -155^{\circ}$.

The detectors were placed at $\pm 170^{\circ}$ relative to the beam direction for the ^{6}Li experiment and at $+165^{\circ}$ and -155° for the ^{7}Li experiment. The corresponding angular apertures were 1.7° and 1.3°, and 0.8° and 0.9°, respectively. Two surface barrier silicon detectors used as monitors were placed at $\pm 30.8^{\circ}$ and $\pm 28.1^{\circ}$ for normalization purposes for ^{6}Li and ^{7}Li, respectively. The uncertainty in the angular positions of the telescopes and monitors were 0.1°. The ratios between the solid angles of the monitors and telescopes were determined by bombarding a gold target at low beam energies, for which the elastic scattering cross section is purely Rutherford. Details of the normalization procedure are found in Ref. [12]. The length of each run was defined such that the number of counts recorded in the elastic peak was of the order of 10 000, corresponding to 1% statistical uncertainties. However, for the backward angles at the highest energies, only a few hundred events were recorded.

Figure 1 shows a typical spectrum for the ^{7}Li + ^{144}Sm system taken at a beam energy of 27 MeV and $\theta_{\rm lab} = -155^{\circ}$. Events corresponding to $Z = 1$, $Z = 2$, and $Z = 3$ could be identified and separated.

Events associated with $Z = 2$ and $Z = 1$ were not used in the subsequent analysis of quasi-elastic processes, since it was not possible to distinguish clearly the corresponding reaction channels, such as NCBU and transfer and evaporation of the CF and ICF (deuteron, tritium, alpha, etc.) compound nuclei. This means that, in fact, the data do not correspond strictly to full quasi-elastic cross section, but rather a lower limit of it, because contributions associated with NCBU and ICF are not taken into account. For this reason, we will define partial QES as the sum of elastic and inelastic scattering and one-neutron transfer channels. Consequently, a direct correspondence to CF cannot be done.

III. QUASI-ELASTIC EXCITATION FUNCTION AND BARRIER DISTRIBUTION FOR THE ^{7}Li + ^{144}Sm SYSTEM

Figure 2 shows the partial QES excitation function for the ^{7}Li + ^{144}Sm system. Figure 3 shows the corresponding

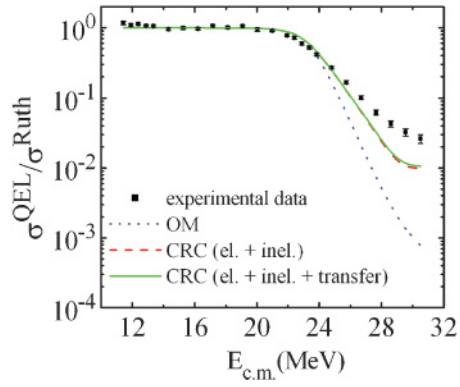

FIG. 2. (Color online) Partial QES excitation function measured at $\theta_{lab} = -155^\circ$ for the ^{7}Li + ^{144}Sm system. The curves are results of CRC calculations that do not take into account the breakup process.

barrier distribution obtained by using Eq. (2). The energy steps correspond to 2 MeV [12] at all energies except at near-barrier energies, where the step is 1 MeV. The center-of-mass energies were corrected by the centrifugal potential at 165° and 155° [5].

To obtain the calculated QES excitation function, the FRESCO code [18] was used throughout this work. As a bare potential, we used the reliable parameter-free double-folding São Paulo potential (SPP) [19,20], which is based on realistic densities [21] and has been able to predict different reaction mechanisms in a wide energy range for several systems [22,23], including fusion barrier distributions for weakly bound systems [24].

It is also important to point out that all theoretical calculations of the barrier distributions were performed using the same three points difference formula at the same energy points for which experimental data were measured, in order to obtain the same systematic errors for both theoretical and experimental barrier distributions.

First we show the results of the coupled reaction channels (CRC) calculations that do not take the breakup channel into account, similar to what has been done for the ^{6}Li + ^{144}Sm system [12]. The results of the calculations for the QES excitation function and barrier distribution are shown in Figs. 2 and 3, respectively, in order to be compared with the experimental values. The curves are the predictions from the SPP with no parameter search. In the CRC calculations, the inelastic and the one-neutron transfer channels were included. The inelastic excitations taken into account were the first two excited states of the ^{144}Sm target ($E^* = 1.66$ MeV, 2^+, $\beta_2 = 0.087$, $r_0 = 1.06$ fm [25]; and $E^* = 1.81$ MeV, 3^-, $\beta_3 = 0.13$, $r_0 = 1.06$ fm [26]) and the first excited state of the ^{7}Li projectile ($E^* = 0.478$ MeV, $1/2^-$, $\beta_2 = 0.71$ [27], $r_0 = 1.06$ fm). The nuclear and Coulomb deformations were assumed to be equal. To include the one-neutron transfer channel, finite range approximation, prior interaction, and full real remnant have been adopted. For the ^{7}Li (g.s.):^{6}Li (g.s.) overlap, the $1p_{3/2}$ and $1p_{1/2}$ components were included, and the spectroscopic factors were taken from Ref. [28] as equal to 0.735 and 0.657, respectively. For the ^{144}Sm (g.s.):^{145}Sm (g.s.) overlap, the spectroscopic factor 0.60 was used [29]. Only transfer to the g.s. of ^{145}Sm was considered, because the Q value for this reaction is −0.493 MeV.

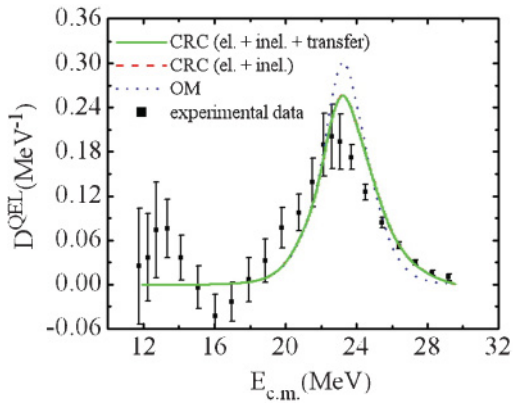

FIG. 3. (Color online) Corresponding partial QES barrier distribution for the ^{7}Li + ^{144}Sm system. The curve is the result of CRC calculations that do not take into account the breakup process.

In Fig. 2, the dotted curve represents the excitation function obtained from optical model calculations. The dashed curve corresponds to the sum of the elastic and all the inelastic cross sections of the target and projectile of the CRC calculation. The full curve, almost superimposed onto the dashed one, results from the addition of the theoretical one-neutron transfer cross section. These calculations suggest that coupling of the one-neutron transfer channel has almost no effect on the excitation function. For this reason, this channel will not be included in the CDCC calculations (see below). Nevertheless, some small influence of the transfer channel coupling on the other reaction mechanisms could be expected.

In Fig. 3, we show the partial QES barrier distribution corresponding to the curves displayed in Fig. 2. Here again the results considering elastic and inelastic scattering (dashed curve) and elastic and inelastic scattering plus one neutron transfer reaction (full curve) are almost undistinguishable from each other. One can observe that neither the excitation function nor the barrier distribution can be well described by these simple calculations. The differences between theoretical calculations and experimental data might be attributed to the influence of the breakup channels, not included in these calculations, on the other reaction mechanisms.

In Figs. 4 and 5, we present the results of full CDCC calculations that take into account the noncapture breakup of the projectile. Although there is recent evidence [30,31] for the occurrence of a two-step transfer-breakup mechanism (i.e., for the present reaction system: ^{7}Li + ^{144}Sm ⇒ ^{6}Li + ^{145}Sm ⇒ ^{2}H + ^{4}He + ^{145}Sm), this process has not been included in our CDCC calculations.

The cluster model was used to represent the interaction of the ^{7}Li weakly bound projectile with the ^{144}Sm target. For the real parts of the ^{3}H + ^{144}Sm and ^{4}He + ^{144}Sm optical potentials, a double-folding potential was used. For the matter densities of the ^{144}Sm target, those of the systematic of the SPP were used. Under the assumption that the matter density and the charge density have similar distributions, we have calculated the matter distribution of the ^{3}H cluster as the sum of the charge distributions of ^{3}H and ^{3}He, which were obtained using the parameters of Ref. [32]. A similar procedure

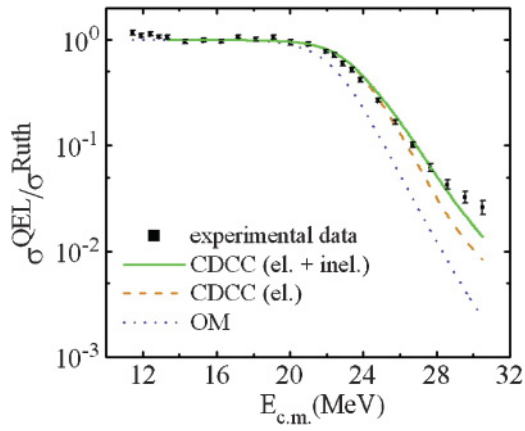

FIG. 4. (Color online) Partial QES excitation function measured at $\theta_{lab} = -155^\circ$ for the ^{7}Li + ^{144}Sm system. The curves are results of CDCC calculations.

was applied for ^{4}He, for which the matter distribution was calculated as twice its charge distribution. The imaginary part of the optical potential was taken as of the Woods-Saxon form with the parameters $W = 50.0$ MeV, $r_w = 1.06$ fm, and $a_w = 0.2$ fm. The choice of these parameters is guided by the incoming wave boundary conditions. The absorption of the flux is supposed to occur only in the inner region of the Coulomb barrier, and the mean free path of the projectile or of the fragments in this region should be less than the potential radius. The results are almost insensitive to the values of these parameters. As we include explicitly the inelastic excitations in the calculations, the choice of imaginary potential inside the barrier avoids possible double counting of the effect of these inelastic excitations on the elastic channel.

To obtain the bin wave functions, the same triton + α scattering potential used in Ref. [33] was adopted. This Woods-Saxon potential with a spin-orbit term guarantees the description of the $7/2^-$ and $5/2^-$ ($L = 3$ coupled to the spin of the triton $s = 1/2$) unbound resonant states. The discretization was done by taking equally spaced bins in momentum breakup subspace for both resonant and nonresonant states following the procedure described in Ref. [33]. The bins are centered

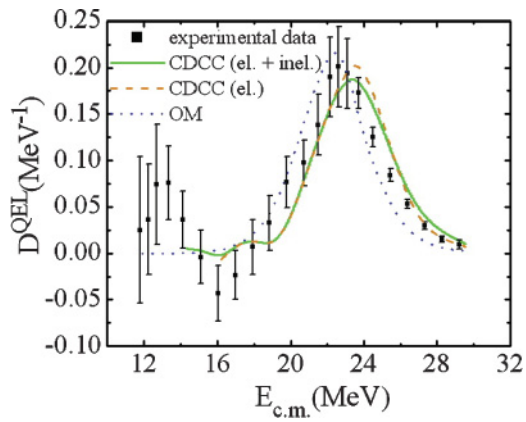

FIG. 5. (Color online) Corresponding partial QES barrier distribution for the ^{7}Li + ^{144}Sm system. The curves are results of CDCC calculations.

at the α-triton relative energies and distributed up to 10 MeV for well above the barrier energy regime. For energies near and well below the Coulomb barrier, the convergence is reached by decreasing the maximum value of bin energy as the ^{7}Li + ^{144}Sm relative energy decreases. At the lowest relative energy ($E_{c.m.} = 13.35$ MeV), the maximum bin energy was $\epsilon_i = 3$ MeV.

The continuum bins were integrated up to $R_{bin} = 190$ fm. The bins were constructed for the relative α-triton orbital angular momentum $0 \leqslant L(\hbar) \leqslant 3$. The main collective states of the target were also included in the coupling scheme (the 2^+ and 3^- states). The deformation parameters of the target were described above. The projectile-target relative motion wave function was integrated numerically up to 500 fm, and it was expanded in partial waves up to $L_{max} = 120\,\hbar$, except for energies larger than $E_{c.m.} = 30.51$ MeV, for which the maximum values of the expansion was $L_{max} = 180\,\hbar$. In all the CDCC calculations, both reorientation and continuum-continuum couplings between ^{7}Li states were considered. This kind of coupling has been shown to be very important in the CDCC cluster model calculations at near-barrier energies [9,34,35]. The importance of the reorientation effects on the elastic scattering was shown by Hnizdo *et al.* in Ref. [36].

In Figs. 4 and 5, the dotted curves are results of uncoupled calculations. The diagonal potential for this optical model calculation is obtained by single folding the ^{3}H + ^{144}Sm plus ^{4}He + ^{144}Sm interactions (both Coulomb and nuclear) over the α-triton g.s. wave function. The dashed curves are the elastic scattering excitation function and barrier distribution obtained from the CDCC calculation that includes only the continuum breakup states. The full curves are results of the full CDCC calculations including, besides the continuum breakup states, the inelastic excitations. Notice that although these cross sections carry the effect of the Coulomb and nuclear breakups, the cross sections of the breakup reactions are not explicitly included in the partial QES cross section used to perform the barrier distribution calculations, since this was not done experimentally. One can observe that a reasonable agreement is obtained for the excitation function and the barrier distribution. The shift of the barrier height of about 1 MeV may arise from the multistep processes not included in the present calculations.

By comparing the dotted and dashed curves of Fig. 5, one can observe that the net effect of the breakup channels is to increase the value of the Coulomb barrier. Thus, according to this calculation, a hindrance of the fusion cross section would be predicted as a consequence of the inclusion of the continuum.

The comparison between the dashed and full curves in either Figs. 4 or 5 reveals that the effect of coupling inelastic excitations of the target is small in the framework of these CDCC calculations, especially at near and below barrier energies. From Fig. 5, it can be seen that the main effect is a slight decrease of the position and the height of the barrier distribution toward a better description of the experimental data. It should be noticed that the effect of the inelastic channels is larger in the case of CRC (see and compare with the equivalent in Figs. 2 and 3). The main reason for this behavior is that when one includes the coupling to the

continuum breakup states, the inelastic channels are affected considerably, because a relevant part of the reaction flux goes to the breakup channels.

By looking at the bare Coulomb barriers of Figs. 3 and 5, represented by dotted curves, one can notice that they are not exactly the same. The reason for this difference lies in the fact that they were calculated with different optical potentials. The barrier of Fig. 3 is obtained by using a double-folding potential of the ^{7}Li projectile and ^{144}Sm target. The one for Fig. 5 was obtained by single folding the interacting potential of the α-^{144}Sm plus triton-^{144}Sm over the ^{7}Li ground state.

IV. QUASI-ELASTIC EXCITATION FUNCTION AND BARRIER DISTRIBUTION FOR THE ^{6}Li + ^{144}Sm SYSTEM

Preliminary calculations were reported for the ^{6}Li + ^{144}Sm system [12] using the SPP as a bare potential, but without coupling channels at the continuum. No agreement was observed between these calculations and the experimental partial QES excitation function and barrier distribution. The discrepancy was attributed to breakup effects not included in the calculations [12].

As for the previous system, the cluster model was used to represent the interaction of the ^{6}Li weakly bound projectile with the ^{144}Sm target. For the real parts of the ^{2}H + ^{144}Sm and ^{4}He + ^{144}Sm optical potentials, a double-folding potential was used. The matter density distribution of the deuteron was obtained following a procedure similar to that described in Sec. III for the α particle, i.e., multiplying by 2 the charge distribution obtained from Ref. [37]. The imaginary part of the optical potentials was the same as for the ^{7}Li + ^{144}Sm system.

To obtain the deuteron + α bin wave functions, we adopted the scattering potential of Ref. [33]. The 3^{+}, 2^{+}, and 1^{+} ($L = 2$ coupled to the spin of the deuteron $s = 1$) unbound resonant states of ^{6}Li were obtained with a Woods-Saxon potential including a spin-orbit term [33]. The details of the bin construction can be found in the same reference.

The maximum energy of the bin energy distribution for this system was 9 MeV for almost all the energy interval. For energies below $E_{\mathrm{c.m.}} = 19.2$ MeV, the maximum energy needed for convergence starts to decrease. For the lowest energy, $E_{\mathrm{c.m.}} = 13.44$ MeV, it was 5 MeV. The continuum bins were integrated up to $R_{\mathrm{bin}} = 160$ fm. For each bin, we considered states with relative α-deuteron orbital angular momentum $0 \leqslant \mathrm{L}(\hbar) \leqslant 3$. The main collective states of the target were also included as for the previous system. The wave function of the projectile-target relative motion was expanded in partial waves up to $L_{\mathrm{max}} = 200\,\hbar$ and calculated numerically up to 500 fm. In all the CDCC calculations, both reorientation and continuum-continuum couplings between ^{6}Li states were considered.

The results of the CDCC calculations are shown in Figs. 6 and 7. The meaning of the curves are the same as in Figs. 4 and 5. From Figs. 6 and 7, we can observe an excellent agreement between the experimental results and the CDCC calculations, without any parameter search.

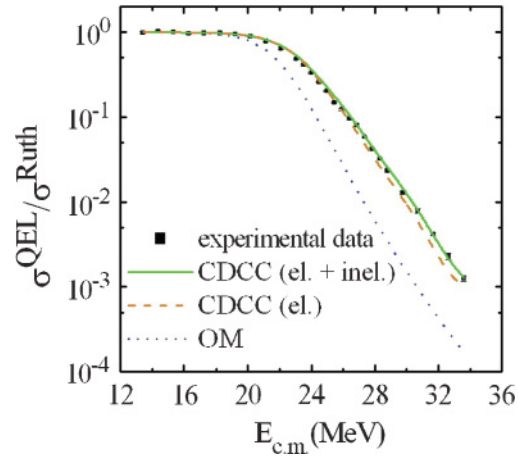

FIG. 6. (Color online) Partial QES excitation function measured at $\theta_{\mathrm{lab}} = 170^{\circ}$ for the ^{6}Li + ^{144}Sm system. The curves are results of CDCC calculations.

By comparing the dotted and dashed curves of Fig. 7, one may notice that the effect of the breakup channel is to increase the value of the Coulomb barrier. The comparison of the curves of Figs. 7 and 5 shows that the effect of the breakup channel is greater for the ^{6}Li + ^{144}Sm system than for the ^{7}Li + ^{144}Sm system. This fact is in agreement with the lower breakup threshold energy for the projectile of the first system. The results obtained switching on and off the inelastic excitations of the target (full and dashed curves, respectively) on Figs. 6 and 7 indicate that the effect of this channel is not very important for the ^{6}Li + ^{144}Sm system. Once again, its effect on the barrier distribution is to slightly decrease its maximum, but in this case it was not enough to change the value of the barrier.

In Ref. [12] it was shown that the inclusion of the resonant 3^{+} state of ^{6}Li on the coupling scheme decreases the barrier considerably. This is expected because of the long half-life of this state, which allows us to consider it as a usual inelastic excited state in the coupling scheme. In the present CDCC calculations, the influence of the inelastic excitations of the target are less important than in the coupled-channel

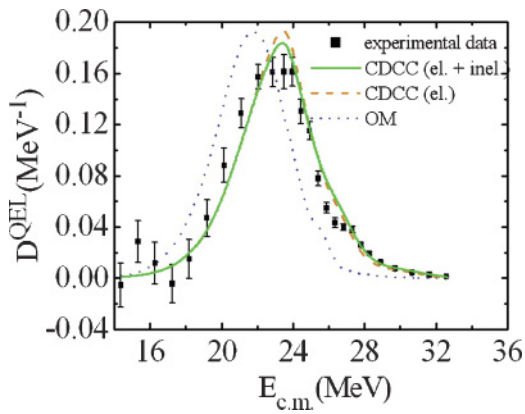

FIG. 7. (Color online) Corresponding partial QES barrier distribution for the ^{6}Li + ^{144}Sm system. The curves are results of CDCC calculations.

calculations performed in Ref. [12]. Indeed, in the present work, we have shown that the net dynamic effect of the coupling to the continuum breakup channels is to increase the Coulomb barrier.

V. SUMMARY AND CONCLUSIONS

We have measured the QES excitation function at backward angle and derived its associated barrier distribution for the ^{7}Li + ^{144}Sm system, and we have reanalyzed previous experimental results for the ^{6}Li + ^{144}Sm system. In the framework of our theoretical calculations and for both studied systems, neither the excitation function nor the associated barrier distribution could be explained without taking into account the breakup process. In fact, the agreement with the experimental data is very good for the ^{6}Li + ^{144}Sm system and reasonable for the ^{7}Li + ^{144}Sm reaction when CDCC calculations are performed. We emphasize that the agreement between data and theoretical results was obtained without using any adjustable parameter in our calculations. The breakup coupling increases the Coulomb barrier of the systems, whereas the coupling of target inelastic excitations seems to be of relatively minor importance.

ACKNOWLEDGMENTS

The authors would like to thank CNPq, FAPERJ, PROSUL, PRONEX, and CONICET for their support.

[1] N. Rowley, G. R. Satchler, and P. H. Stelson, Phys. Lett. **B254**, 25 (1991).
[2] M. Dasgupta *et al.*, Annu. Rev. Nucl. Part. Sci. **48**, 401 (1998), and references therein.
[3] J. R. Leigh *et al.*, Phys. Rev. C **52**, 3151 (1995).
[4] A. T. Kruppa, E. Romain, M. A. Nagarajan, and N. Rowley, Nucl. Phys. **A560**, 845 (1993).
[5] H. Timmers *et al.*, Nucl. Phys. **A584**, 190 (1995).
[6] N. Rowley *et al.*, Phys. Lett. **B373**, 23 (1996).
[7] H. Timmers *et al.*, Phys. Lett. **B399**, 35 (1997).
[8] H. Timmers *et al.*, Nucl. Phys. **A633**, 421 (1998).
[9] L. F. Canto, P. R. S. Gomes, R. Donangelo, and M. S. Hussein, Phys. Rep. **424**, 1 (2006), and references therein.
[10] M. Dasgupta *et al.*, Phys. Rev. Lett. **82**, 1395 (1999); Phys. Rev. C **66**, 041602(R) (2002); **70**, 024606 (2004).
[11] C. J. Lin *et al.*, Nucl. Phys. **A787**, 281c (2007).
[12] D. S. Monteiro *et al.*, Phys. Rev. C **79**, 014601 (2009).
[13] S. Mukherjee *et al.*, Phys. Rev. C **80**, 014607 (2009).
[14] J. Lubian, T. Correa, P. R. S. Gomes, and L. F. Canto, Phys. Rev. C **78**, 064615 (2008).
[15] P. R. S. Gomes *et al.*, Phys. Rev. C **73**, 064606 (2006); Phys. Lett. **B634**, 356 (2006).
[16] P. K. Rath *et al.*, Phys. Rev. C **79**, 051601(R) (2009).
[17] R. H. Spear *et al.*, Nucl. Instrum. Methods **147**, 455 (1977).
[18] I. J. Thompson, Comput. Phys. Rep. **7**, 167 (1988) and www.fresco.org.uk.
[19] L. C. Chamon *et al.*, Phys. Rev. C **66**, 014610 (2002).
[20] M. A. G. Alvarez *et al.*, Nucl. Phys. **A723**, 93 (2003).
[21] C. P. Silva *et al.*, Nucl. Phys. **A679**, 287 (2001).
[22] L. R. Gasques, L. C. Chamon, P. R. S. Gomes, and J. Lubian, Nucl. Phys. **A764**, 135 (2006).
[23] J. J. S. Alves *et al.*, Nucl. Phys. **A748**, 59 (2005).
[24] E. Crema, L. C. Chamon, and P. R. S. Gomes, Phys. Rev. C **72**, 034610 (2005).
[25] S. Raman, C. W. Nestor Jr., and P. Tikkanena, At. Data Nucl. Data Tables **78**, 1 (2001).
[26] T. Kibédi and R. H. Spear, At. Data Nucl. Data Tables **80**, 35 (2002).
[27] J. Lubian *et al.*, Nucl. Phys. **A791**, 24 (2007).
[28] A. A. Rudchik *et al.*, Phys. Rev. C **72**, 034608 (2005).
[29] S. T. Thornton *et al.*, Phys. Rev. C **12**, 877 (1975).
[30] A. Shrivastava *et al.*, Phys. Lett. **B633**, 463 (2006).
[31] D. Martinez Heimann *et al.*, AIP Conf. Proc. **1139**, 11 (2009).
[32] H. Devries, C. W. Dejager, and C. Devries, At. Data Nucl. Data Tables **36**, 495 (1987).
[33] A. Diaz-Torres, I. J. Thompson, and C. Beck, Phys. Rev. C **68**, 044607 (2003).
[34] N. Keeley, K. W. Kemper, and K. Rusek, Phys. Rev. C **66**, 044605 (2002).
[35] N. Keeley, R. Raabe, N. Alamanos, and J. L. Sida, Prog. Part. Nucl. Phys. **59**, 579 (2007).
[36] V. Hnizdo, K. W. Kemper, and J. Szymakowski, Phys. Rev. Lett. **46**, 590 (1981).
[37] D. Abbott *et al.*, Eur. Phys. J. A **7**, 421 (2000).